A general procedure for deriving thin plate bending elements with one degree of freedom per node

E. Oñate
M. Cervera

Publicación CIMNE Nº 32, April 1993

A general procedure for deriving thin plate bending elements with one degree of freedom per node

E. Oñate
M. Cervera

Publicación CIMNE Nº 32, April 1993

To be published in Engineering Computations

Centro Internacional de Métodos Numéricos en Ingeniería
Gran Capitán s/n, 08034 Barcelona, España

A general procedure for deriving thin plate bending elements with one degree of freedom per node

E. Oñate
M. Cervera

E.T.S. Ingenieros de Caminos, Canales y Puertos
Universidad Politécnica de Catalunya
Gran Capitán s/n, 08034 Barcelona, Spain

Summary

A general methodology for deriving thin plate bending elements with a single degree of freedom per node is presented. The formulation is based on the combination of a standard C_0 finite element interpolation for the deflection field with an independent approximation of the curvatures which are expressed in terms of the deflection gradient along the sides using a finite volume-like approach. The formulation is particularized for the simplest element of the family, i.e. the three node triangle with three degrees of freedom. The potential of the new element is shown through different examples of application.

INTRODUCTION

This paper deals with the development of thin plate bending finite elements using only out-of-plane translational nodal degrees of freedom. Indeed, these elements could be very advantageous over more traditional and complex plate elements, especially in the field of large size nonlinear problems in statics and dynamics.

The idea of using the deflection as the only variable for plate bending analysis is not new and most Finite Difference (FD) procedures are based on this approach [1], [11]. The obvious difficulties of FD techniques are the treatment of boundary conditions and the problems for dealing with non-orthogonal or unstructured grids.

Several authors have tried to derive finite elements with the lateral deflection as the only nodal variable. So far the methods proposed limit their applicability to triangular element shapes only. Barnes [2] proposed a method for deriving a three node triangle with 3 nodal degrees of freedom (DOF) based on the computation of the curvatures in terms of the normal rotations at the mid-side points

determined from the nodal deflections of adjacent elements. This method has been extended by Hampshire et al. [3] assuming that the elements are hinged together at their common boundaries, the bending stiffness being represented by torsional springs resisting the rotations about the hinge lines. More recently, Phaal and Calladine [4], [5] have proposed a similar class of triangles for plate and flat shell analysis. The derivation of these elements is based on the concept of "overlapping hinged bending elements". The basic idea is to represent the deflection field using a complete quadratic polynomial defined over the six nodes patch formed by three elements which can thus be considered as a six node macro-element. This procedure requires a careful identification of the element patches, and it involves the inversion of a 3×3 matrix for each patch. Also, fictitious external nodes are needed to impose the boundary conditions at the plate edges.

In this paper an alternative methodology for deriving thin plate bending elements with a single degree of freedom per node is presented. The formulation is based on the interpolation of the deflection field inside each element using a C_0 approximation. An independent assumed curvature field is then chosen and this is related to the deflection gradient (i.e. the rotations) along the sides using a finite volume-like approach. Finally, the deflection gradient along the sides is computed in terms of the nodal deflections of adjacent elements in a straight-forward manner.

The formulation proposed is completely general and it allows to derive thin plate bending elements with a single degree of freedom per node of triangular and quadrilateral shapes with different approximations. For the sake of conciseness only the simplest element of the family, i.e. the three node triangle with three degrees of freedom will be derived and assessed in detail here.

The layout of the paper is the following. In next section the basic ideas of the formulation proposed are presented in their general form. Then the formulation is particularized to the development of a simple three node triangular element with only three nodal degrees of freedom. Details of the derivation of the element stiffness matrix and the load vector, the imposition of boundary conditions and the evaluation of stress resultants are also given. Finally, the efficiency of the new element is checked with some examples of application.

BASIC THEORY

Let us consider a plate with the sign criterion for the vertical deflection w and the rotations θ_x,θ_y as shown in Figure 1. We will assume Kirchhoff's orthogonality conditions for thin plate analysis to hold, i.e.,

$$\theta_x = \frac{\partial w}{\partial x} \qquad \text{and} \qquad \theta_y = \frac{\partial w}{\partial y} \tag{1}$$

Under these conditions the curvature field can be expressed as [11]

$$\boldsymbol{\kappa} = \left[\kappa_x, \kappa_y, \kappa_{xy}\right]^T = \left[-\frac{\partial^2 w}{\partial x^2}, -\frac{\partial^2 w}{\partial y^2}, -2\frac{\partial^2 w}{\partial x \partial y}\right]^T = \mathbf{L}w \tag{2a}$$

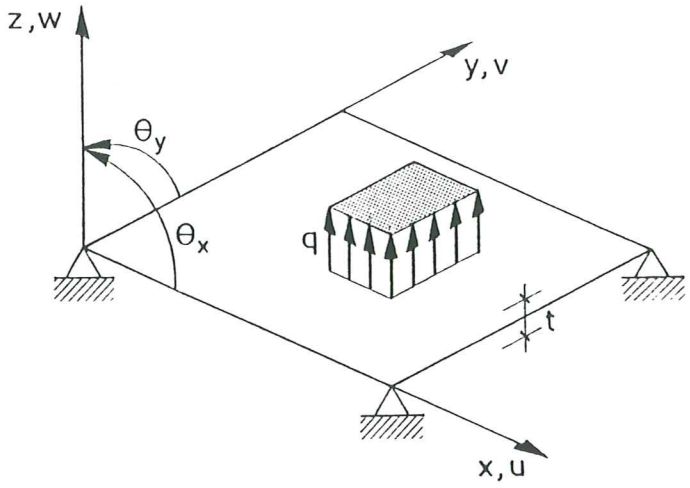

Figure 1 Sign convenion for the deflection and the rotations in a plate

with the differential operator $\mathbf{L}$ defined as

$$\mathbf{L} = \left[-\frac{\partial^2}{\partial x^2}, -\frac{\partial^2}{\partial y^2}, -2\frac{\partial^2}{\partial x \partial y} \right]^T \tag{2b}$$

The constitutive relationship between bending moments and curvatures can be written as

$$\mathbf{m} = [M_x, M_y, M_{xy}]^T = \mathbf{D}\boldsymbol{\kappa} \tag{3}$$

with

$$\mathbf{D} = \frac{Et^3}{12(1-\nu^2)} \begin{bmatrix} 1 & \nu & 0 \\ \nu & 1 & 0 \\ 0 & 0 & \frac{1-\nu}{2} \end{bmatrix} \tag{4}$$

where E and ν are the Young's modulus and the Poisson's ratio, respectively. The sign criterion for bending moments can be seen in Figure 2.

The Principle of Virtual Work (PVW) is written in its simpler form as

$$\int\int_A \delta\boldsymbol{\kappa}^T \mathbf{m} dA = \int\int_A \delta w q dA \tag{5}$$

where virtual curvatures $\delta\boldsymbol{\kappa}$ and virtual deflections δw are related by $\delta\boldsymbol{\kappa} = \mathbf{L}\delta w$, A is the area of the plate and q the intensity of an uniformly distributed vertical load.

Mixed formulation

The PVW can be rewritten substituting Eq.(3) into Eq.(5) to give

$$\int\int_A \delta\boldsymbol{\kappa}^T \mathbf{D}\boldsymbol{\kappa} dA = \int\int_A \delta w q dA \tag{6}$$

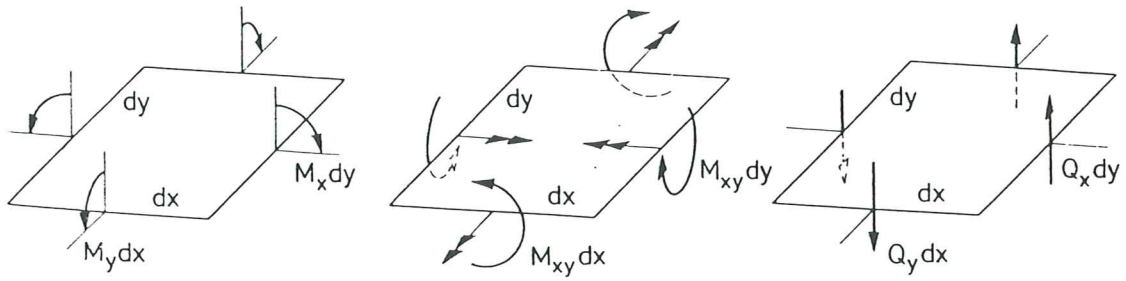

Figure 2 Sign criterion for bending moments and shear forces in a plate element

Eq.(2a) can be written in integral form using the method of weighted residuals to give

$$\int\int_A \mathbf{W}^T [\boldsymbol{\kappa} - \mathbf{L}w]\, dA = 0 \tag{7a}$$

where

$$\mathbf{W} = \begin{bmatrix} W_1 & 0 & 0 \\ 0 & W_2 & 0 \\ 0 & 0 & W_3 \end{bmatrix} \tag{7b}$$

with W_i being arbitrary weighting functions.

Eq.(7) can be simplified by making

$$W_i(\mathbf{x}) = \begin{cases} 1 & \mathbf{x} \in A_s \\ 0 & \mathbf{x} \notin A_s \end{cases} \tag{7c}$$

where A_s is an arbitrary subdomain of the plate, and then integrating by parts the term involving the deflection to give

$$\int\int_{A_s} \boldsymbol{\kappa} dA = \int_{\Gamma_s} \mathbf{T}\boldsymbol{\nabla} w d\Gamma \tag{8}$$

where

$$\mathbf{T} = \begin{bmatrix} n_x & 0 \\ 0 & n_y \\ n_y & n_x \end{bmatrix} \quad , \quad \boldsymbol{\nabla} = \begin{Bmatrix} \frac{\partial}{\partial_x} \\ \frac{\partial}{\partial_y} \end{Bmatrix} \tag{9}$$

and Γ_s is the boundary of the subdomain A_s.

Eqs. (6) and (8) are the basis for the finite element discretization presented in the next section.

Remark 1. The choice of W_i leading to Eq.(8) is typical of finite volume methods (FVM), extensively used in thermal and fluid flow problems [6], [7],

[10].For a recent discussion of the FVM in the context of structural mechanics see references [8] and [9].

Remark 2. Note that Eq.(8) is satisfied for any patch of area A_s surrounded by a boundary Γ_s.

Remark 3. Note also that Eq.(8) involves the computation of the deflection gradient along the boundary Γ_s of the subdomain considered. This poses some difficulties when a C_0 finite element approximation is used for the deflection, as this leads to a discontinuous gradient of w across boundaries of adjacent elements. This problem can be overcome by computing the deflection gradient in an element boundary as the average of the gradients contributed by the two elements sharing the boundary. More details of this averaging procedure are given in the next section.

FINITE ELEMENT DISCRETIZATION

The plate is discretized in a mesh of C_0 finite elements in the standard form [12], [13]. The deflection field is written in terms of the nodal deflections as

$$w = \sum_{i=1}^{n} N_{w_i} \bar{w}_i = \mathbf{N}_w \bar{\boldsymbol{w}} \tag{10}$$

where $\bar{w}_i$ are nodal deflection values, $\bar{\boldsymbol{w}} = [\bar{w}_1, \ldots, \bar{w}_n]^T$, N_{w_i} is the shape function of node i and n is the number of nodes in the mesh.

The three curvatures can now be interpolated over the mesh using a C_0 continuous approximation as

$$\boldsymbol{\kappa} = \sum_{i=1}^{p} N_{\gamma_i} \mathbf{I}_3 \bar{\boldsymbol{\kappa}}_i = \mathbf{N}_\gamma \bar{\boldsymbol{\kappa}} \tag{11}$$

where p is the total number of interpolating points in the mesh; $\bar{\boldsymbol{\kappa}}_i$ are the curvature values at the i-th interpolating point; N_{γ_i} is the curvature interpolating function for point i; $\mathbf{I}_3$ is the 3×3 unit matrix and

$$\mathbf{N}_\gamma = [N_{\gamma_i}\mathbf{I}_3, \ldots, N_{\gamma_p}\mathbf{I}_3] \quad ; \quad \bar{\boldsymbol{\kappa}} = [\bar{\boldsymbol{\kappa}}_1^T, \ldots \bar{\boldsymbol{\kappa}}_p^T]^T \tag{12}$$

Substitution of Eqs. (10) and (11) in Eq. (8) gives

$$\left[\int\int_{A_i} \mathbf{N}_\gamma d\Omega \right] \bar{\boldsymbol{\kappa}} = \left[\int_{\Gamma_i} \mathbf{T} \nabla \mathbf{N}_w \right] \bar{\boldsymbol{w}} \qquad i = 1, \ldots, p \tag{13}$$

where A_i and Γ_i are respectively the area and the boundary corresponding to the "domain" associated with the i-th curvature interpolating point (see Remark 3).

Eq.(13) can be written in matrix form as

$$\mathbf{P}\bar{\boldsymbol{\kappa}} = \mathbf{H}\bar{\boldsymbol{w}} \tag{14}$$

where $\mathbf{P}$ and $\mathbf{H}$ are $3p \times 3p$ and $3p \times n$ matrices respectively, given by

$$\mathbf{P}_{ij} = \int\int_{A_i} N_{\gamma_j} \mathbf{I}_3 d\Omega \tag{15a}$$

$$\mathbf{H}_{ij} = \int_{\Gamma_i} \mathbf{T}(\nabla N_{w_j}) d\Gamma \tag{15b}$$

Eq.(14) allows to obtain the discrete curvature variables in terms of the nodal deflections as

$$\bar{\boldsymbol{\kappa}} = \mathbf{P}^{-1}\mathbf{H}\bar{\boldsymbol{w}} \tag{16}$$

Substituting Eq.(16) into Eq.(11) yields

$$\boldsymbol{\kappa} = \mathbf{B}\bar{\boldsymbol{w}} \tag{17}$$

where the "strain matrix" $\mathbf{B}$ is given by

$$\mathbf{B} = \mathbf{N}_\gamma \mathbf{P}^{-1}\mathbf{H} \tag{18}$$

A similar procedure can be followed to obtain the relationship between virtual curvatures and virtual deflections as

$$\delta\boldsymbol{\kappa} = \mathbf{B}\delta\bar{\boldsymbol{w}} \tag{19}$$

where $\mathbf{B}$ coincides with that of Eq. (18).

Substituting Eqs.(10), (17) and (19) into Eq.(6) allows to derive the global matrix equilibrium equations for the plate in the standard form

$$\mathbf{K}\bar{\boldsymbol{w}} = \mathbf{f} \tag{20}$$

where the stiffness matrix and the equivalent nodal force vector for the whole mesh are given by

$$\mathbf{K} = \int\int_A \mathbf{B}^T \mathbf{D}\mathbf{B} dA \tag{21a}$$

$$\mathbf{f} = \int\int_A \mathbf{N}_w^T q dA \tag{21b}$$

Remark 4. There are multiple options to define the area A_i and the boundary Γ_i of the "domain" associated to each curvature interpolating point, and here again the finite volume methodology can be used [8], [9]. Figure 3 shows some alternatives based on the assumption that $p = n$, i.e, the curvature interpolating points coincide with the nodes and thus $N_{\gamma_i} = N_{w_i}$. Note that in the so-called "vertex centered" approach the computation of the deflection

gradients along interelemental sides requires the adequate averaging of the gradients contributed from the two element sharing the side, as mentioned in Remark 2. This aspect will be further detailed later.

Remark 5. The fields $\boldsymbol{w}$ and $\boldsymbol{\kappa}$ must satisfy certain compatibility conditions which ensure the existence of the solution for the mixed problem [12]. These conditions can be summarized as

$$n_{\bar{\kappa}} \geq n_{\bar{w}} \tag{22}$$

where $n_{\bar{\kappa}}$ and $n_{\bar{w}}$ denote the number of available degrees of freedom for the curvature and deflection fields (after discounting the prescribed values). The proof of this condition can be seen in the Appendix.

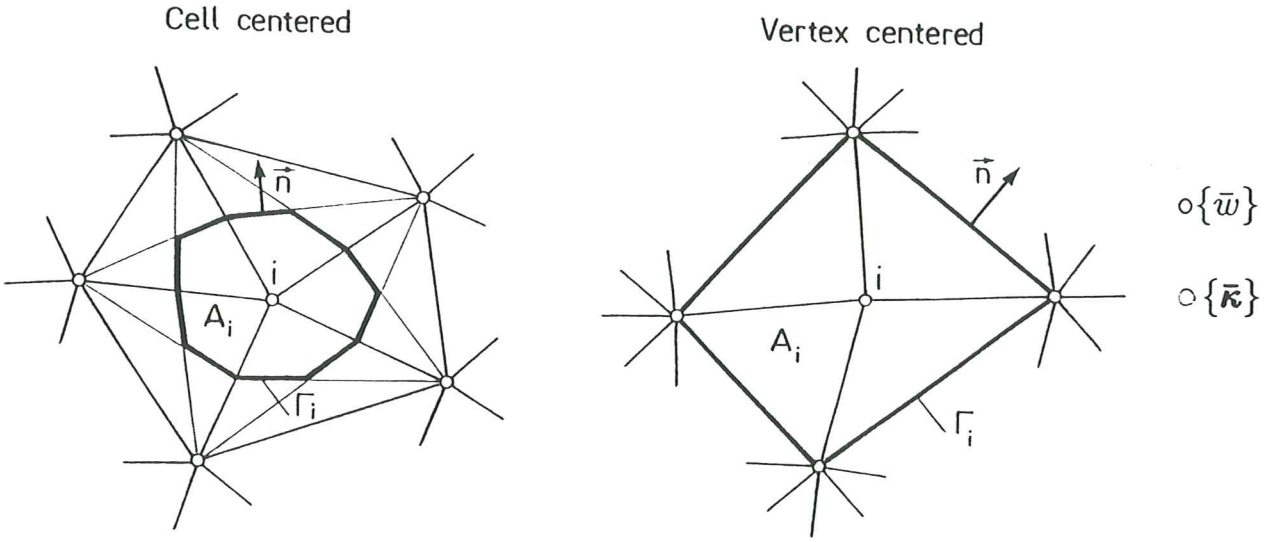

Figure 3 Cell centered and vertex centered domains surrounding a node i

DISCONTINUOUS APPROXIMATION OF THE CURVATURES FIELD

The procedure presented above requires the inversion of the global matrix $\mathbf{P}$ and this can be expensive for practical purposes. A way to overcome this difficulty is to define a discontinuous approximation of the curvatures field. Thus Eq.(11) can be written individually for each element as

$$\boldsymbol{\kappa}^{(e)} = \sum_{i=1}^{n_c} N_{\gamma_i}^{(e)} \mathbf{I}_3 \bar{\boldsymbol{\kappa}}_i^{(e)} = \mathbf{N}_{\gamma}^{(e)} \bar{\boldsymbol{\kappa}}^{(e)} \tag{23}$$

where n_c is the number of curvature interpolating points within element e; $N_{\gamma_i}^{(e)}$ are *discontinuous* shape functions and all other terms of Eq.(23) have the same meaning as in Eq.(11), but now they are referred to an individual element.

Eq.(8) can now be particularized for an individual element to give

$$\int\int_{A_i^{(e)}} \kappa^{(e)} dA = \int_{\Gamma_i^{(e)}} \mathbf{T}\nabla w^{(e)} d\Gamma \tag{24}$$

where $A_i^{(e)}$ and $\Gamma_i^{(e)}$ are now the area and the boundary of the domain associated to the i-th curvature interpolating point within the element. Some examples of typical "vertex-centered domains" for piece-wise constant and linear discontinuous curvature interpolations in triangular and quadrilateral elements are shown in Figure 4.

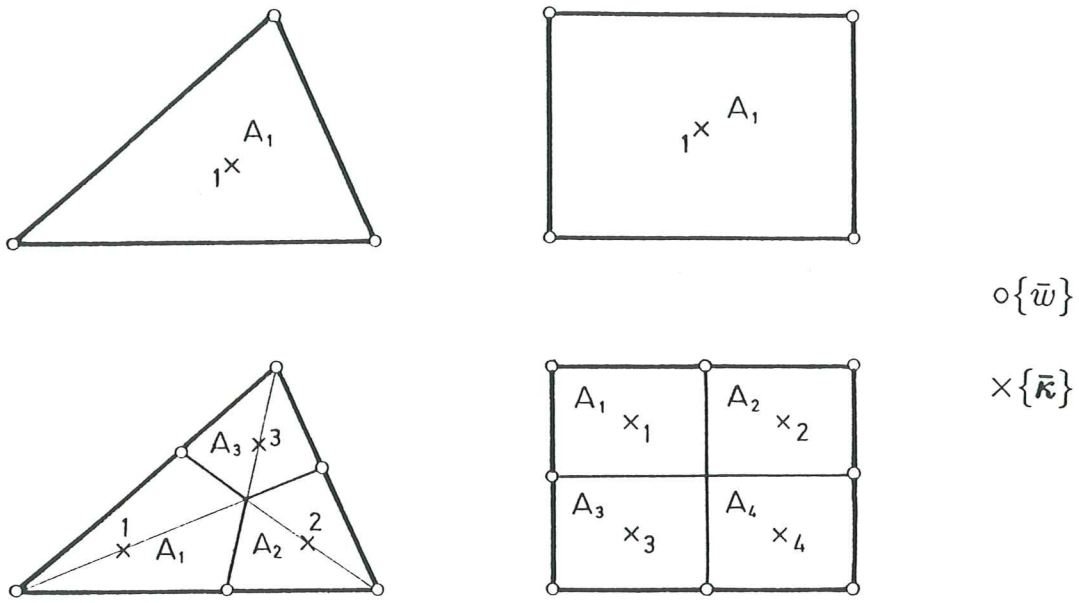

Figure 4 Typical vertex-centered domain for piece-wise constant and linear discontinuous curvatures interpolations over triangles and rectangles

Eq.(24) requires necessarily the computation of the deflection gradient along the element sides. This poses some difficulties due to the discontinuous nature of the term ∇w between elements. As mentioned earlier, a simple method to overcome this problem is to compute the deflection gradient at a point of an element side as the average value of the gradients contributed to the point from the two elements sharing that particular side. Thus, the computation of the r.h.s. of Eq.24) for each element involves necessarily the nodes included in the patch formed by this element and all adjacent elements. Figure 5 shows typical patches associated to linear triangular and bilinear quadrilateral elements with a single curvature interpolating point using a vertex centered type approach.

Substituting Eqs.(10) and (23) into Eq.(24) allows to relate the element curvature variables to the nodal deflections of the patch associated to each element as

$$\mathbf{P}^{(e)}\bar{\boldsymbol{\kappa}}^{(e)} = \mathbf{H}^{(e)}\mathbf{a}^{(e)} \tag{25}$$

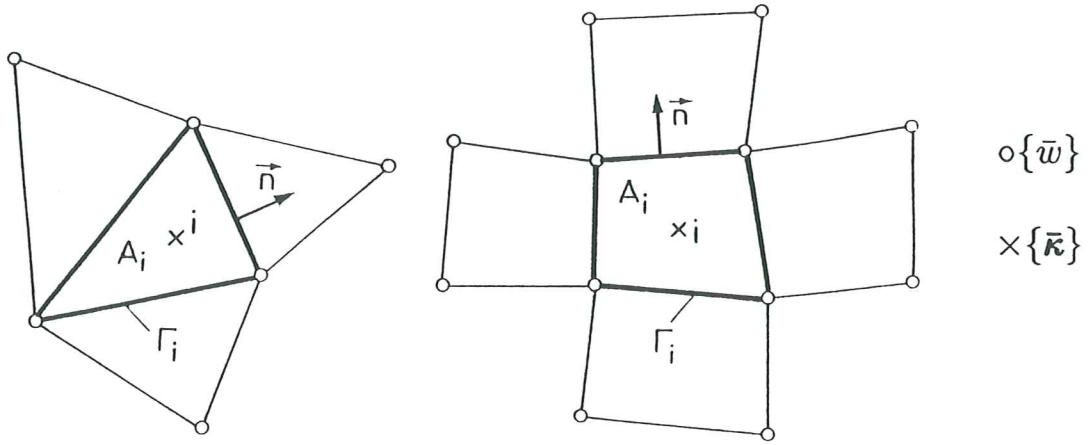

Figure 5 Typical patches associated to linear triangular and bilinear quadrilateral elements with a single curvature interpolating point (vertex-centered approach)

where $\mathbf{a}^{(e)} = [\bar{w}_1, \bar{w}_2, \ldots \bar{w}_{n_p}]^T$ and n_p is the number of nodes involved in the patch formed by element e and all adjacent elements sharing the sides of this element.

Matrices $\mathbf{P}^{(e)}$ and $\mathbf{H}^{(e)}$ are obtained as

$$\mathbf{P}_{ij}^{(e)} = \int\int_{A_i^{(e)}} N_{\gamma_j} \mathbf{I}_3 dA \qquad i = 1, \ldots, n_c \;\; ; \;\; j = 1, \ldots, n_c \tag{26}$$

$$\mathbf{H}_{ij}^{(e)} = \int_{\Gamma_i^{(e)}} \mathbf{T} \left[\alpha \nabla N_{w_j}^{(e)} + \beta \nabla N_{w_j}^{(f)} \right] d\Gamma \qquad i = 1, \ldots, n_c \;\; ; \;\; j = 1, \ldots, n_p \tag{27}$$

where $\alpha = 1$ and $\beta = 0$ for the part of the domain boundary $\Gamma_i^{(e)}$ located within the element, and $\alpha = \beta = \frac{1}{2}$ for the part of $\Gamma_i^{(e)}$ coinciding with the side shared by element e and an adjacent element f.

In Eq.(27) $N_{w_j}^{(e)}$ denotes, as usual, the shape function of node j defined locally over element e.

Remark 6. Note that if a single curvature interpolating point at the element mid-point is used, the domain area and its boundary coincide with the element area and its boundary, respectively, i.e. $A_i^{(e)} = A^{(e)}$ and $\Gamma_i^{(e)} = \Gamma^{(e)}$ (see Figures 3 and 4).

Remark 7. The simple averaging procedure for estimation of the deflection derivative along the sides could be obviously improved by using more sophisticated derivative approximation procedures. Here the use of special smoothing techniques [15], derivative recovery methods [16] or diffuse approximation [17] could prove to be advantageous and they should be explored.

The discontinuous nature of the curvatures field allows to eliminate the element curvature variables $\bar{\boldsymbol{\kappa}}^{(e)}$ in terms of the nodal deflection of the patch from Eq.(25) as

$$\bar{\boldsymbol{\kappa}}^{(e)} = \left[\mathbf{P}^{(e)} \right]^{-1} \mathbf{H}^{(e)} \mathbf{a}^{(e)} \tag{28}$$

The curvature matrix for the element is finally obtained substituting Eq. (28) into Eq.(23) to give

$$\boldsymbol{\kappa}^{(e)} = \mathbf{N}_{\gamma}^{(e)} \left[\bar{\mathbf{P}}^{(e)}\right]^{-1} \mathbf{H}^{(e)} \mathbf{a}^{(e)} = \mathbf{B}^{(e)} \mathbf{a}^{(e)} \tag{29}$$

with

$$\mathbf{B}^{(e)} = \mathbf{N}_{\gamma}^{(e)} \left[\mathbf{P}^{(e)}\right]^{-1} \mathbf{H}^{(e)} \tag{30}$$

Substituting Eq.(30) into Eq.(6) yields the discretized equilibrium equations for the element in terms of the "patch" nodal deflection variables $\mathbf{a}^{(e)}$ in the standard form [13] as

$$\mathbf{K}^{(e)} \mathbf{a}^{(e)} - \mathbf{f}^{(e)} = \mathbf{q}^{(e)} \tag{31}$$

where $\mathbf{q}^{(e)}$ are the equilibrating nodal forces needed for global assembly purposes only and the stiffness matrix and the equivalent nodal force vector for the element are given by

$$\mathbf{K}^{(e)} = \int\int_{A^{(e)}} \left[\mathbf{B}^{(e)}\right]^{T} \mathbf{D} \mathbf{B}^{(e)} dA \tag{32}$$

$$\mathbf{f}^{(e)} = \int\int_{A^{(e)}} \left[\mathbf{N}^{(e)^{T}}, \mathbf{0}, \ldots, \mathbf{0}\right] q dA \tag{33}$$

The columns of zeros in vector $\mathbf{f}^{(e)}$ take into account the effect of the patch elements adjacent to element e, which obviously should not contribute to the nodal forces of this element.

The global equilibrium equations are obtained by assembly of the element contributions in the standard manner [12], [13].

Remark 8. Note that the equilibrium equation (31) for the element involve the nodal deflection variables of the patch formed by element e and all adjacent elements sharing the sides of that element. This naturally leads to a wider bandwidth in the global equations system after assembly than that arising from the standard finite element method.

The procedure presented is completely general and it allows to derive plate bending elements with a single degree of freedom per node of quadrilateral and triangular shapes of any order. To clarify concepts the formulation will be particularized next to derive the simplest element of the family, i.e., the three node triangle with only 3 degrees of freedom, which shows a promising behaviour for plate analysis.

DERIVATION OF A THREE NODE TRIANGULAR PLATE ELEMENT WITH 3 DOF

The geometry of the element is shown in Figure 6 , where the patch of elements surrounding a particular element e with nodes i, j, k is shown.

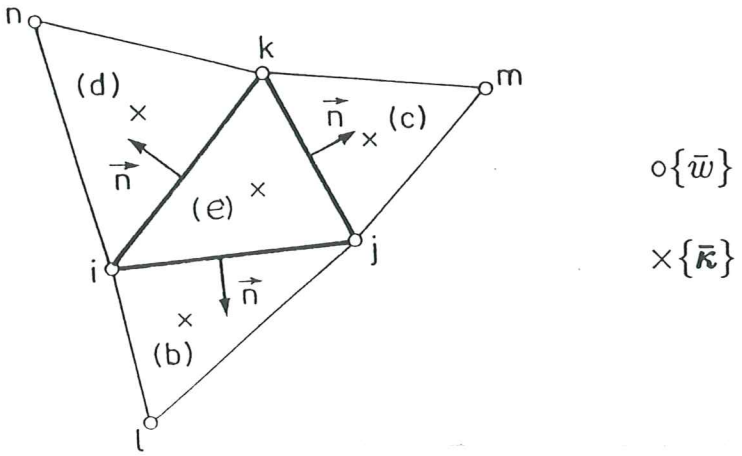

Figure 6 Patch of three node triangles associated to a vertex-centered domain i, j, k

The deflection field is linearly interpolated within each element using standard linear shape functions of the form

$$N_i^{(e)} = \frac{1}{2A^{(e)}}(a_i^{(e)} + b_i^{(e)}x + c_i^{(e)}y) \tag{34a}$$

where

$$a_i^{(e)} = x_j y_k - x_k y_j \ , \ b_i^{(e)} = y_j - y_k \ , \ c_i^{(e)} = x_k - x_j \tag{34b}$$

and x_i, y_i, etc. are the coordinates of the element nodes. The superindex (e) is needed in $a_i^{(e)}$, etc. since node i can be shared by different elements.

The curvature field within each element is now expressed using a piece-wise constant approximation, i.e. $N_{\gamma_i}^{(e)} = 1$ in Eq.(23), which naturally gives from Eq.(26)

$$\mathbf{P}^{(e)} = A^{(e)}\mathbf{I}_3 \tag{35}$$

As mentioned earlier, this curvature approximation corresponds to a vertex-centered approach in which the "domain" surrounding each curvature interpolating point coincides with that of a single element.

The derivation of matrix $\mathbf{H}^{(e)}$ follows the lines explained in the previous section. This involves a simple procedure if we first note that the external unit normal vector to a side ij of length l_{ij} (see Figure 5) is given by

$$\mathbf{n} = \frac{1}{l_{ij}} \left[y_{ij}, -x_{ij} \right]^T \tag{36a}$$

with

$$y_{ij} = y_i - y_j \quad , \quad x_{ij} = x_i - x_j \tag{36b}$$

The line integrals along the element sides of some characteristic terms of Eq.(27) are simply expressed in terms of "patch" variables following the averaging procedure explained in the previous section. Thus, for side ij we have

$$\int_{l_{ij}} n_x \frac{\partial w}{\partial x} d\Gamma = \frac{y_{ij}}{2} \left[(\bar{b}_i^{(e)} + \bar{b}_i^{(b)}), (\bar{b}_j^{(e)} + \bar{b}_j^{(b)}), \bar{b}_k^{(e)}, \bar{b}_l^{(b)}, 0, 0 \right] \mathbf{a}^{(e)} \tag{37}$$

$$\int_{l_{ij}} n_y \frac{\partial w}{\partial y} d\Gamma = -\frac{x_{ij}}{2} \left[(\bar{c}_i^{(e)} + \bar{c}_i^{(b)}), (\bar{c}_j^{(e)} + \bar{c}_j^{(b)}), \bar{c}_k^{(e)}, \bar{c}_l^{(b)}, 0, 0 \right] \mathbf{a}^{(e)} \tag{38}$$

where

$$\bar{b}_i^{(e)} = \frac{b_i^{(e)}}{2A^{(e)}} \quad , \quad \bar{c}_i^{(e)} = \frac{c_i^{(e)}}{2A^{(e)}} \quad , \quad \text{etc.} \tag{39}$$

and

$$\mathbf{a}^{(e)} = \left[w_i, w_j, w_k, w_l, w_m, w_n \right]^T \tag{40}$$

is the nodal deflections vector of the four elements patch corresponding to element e. A similar expression can be obtained for the integral $\int_{l_{ij}} \left(n_y \frac{\partial w}{\partial x} + n_x \frac{\partial w}{\partial y} \right) d\Gamma$. The derivation of matrix $\mathbf{H}^{(e)}$ of Eq.(30) is straight-forward and its explicit form is given in Table 1.a.

The curvature matrix for the element is obtained using Eq.(30). The simple curvature approximation chosen for the element allows to write

$$\mathbf{B}^{(e)} = \frac{1}{A^{(e)}} \mathbf{H}^{(e)} \tag{41}$$

The stiffness matrix for the element is then simply obtained (for homogeneous material properties) as

$$\mathbf{K}^{(e)} = \frac{1}{A^{(e)}} \left[\mathbf{H}^{(e)} \right]^T \mathbf{D} \mathbf{H}^{(e)} \tag{42}$$

and the equivalent nodal force for an uniformly distributed load of intensity q is

$$\mathbf{f}^{(e)} = \frac{q A^{(e)}}{3} [1, 1, 1, 0, 0, 0]^T \tag{43}$$

The global equilibrium equations are assembled in the standard manner from the element contributions, taking into account that the equation for an individual element relate the six nodal deflection variables of the corresponding four elements patch.

Remark 9. An alternative procedure for deriving matrix $\mathbf{H}^{(e)}$ can be based in the definition of the deflection gradients along a side in terms of the *tangential* and *normal rotations* along that side. Since the tangential rotations are continuous along the side $\left(\text{i.e. } \frac{\partial w}{\partial s}|_{ij} = \frac{w_j - w_i}{l_{ij}}\right)$ only the normal rotations need to be averaged using the values from the two adjacent elements. For shortness reasons the 3 DOF plate triangle above derived will be termed hereonwards BPT (for Basic Plate Triangle) element.

IMPOSITION OF THE BOUNDARY CONDITIONS

The practical application of the plate bending element described above requires the consideration of the various types of boundary conditions which are usual in plate bending analysis, that is, free edges, simply supported edges, clamped edges and fictitious symmetry edges.

A plate bending element which lies along a boundary belongs to a "patch" where one of the contributing elements is missing (see Figure 7). For the purpose of derivation let us suppose that the element edge along the boundary is Γ_{ij}, and so, element b and node l are the ones missing in the corresponding patch. In this situation, a possible expression to compute the deflection gradient along the boundary side Γ_{ij} is

$$\nabla w|_{\Gamma_{ij}} = \nabla w^{(e)}|_{\Gamma_{ij}} \tag{44}$$

In practice this implies making $\alpha = 1$ and $\beta = 0$ in Eq.(27) for the part of the line integral over $\Gamma_i^{(e)}$ coinciding with Γ_{ij}.

Remark 10. This approximation can be obviously used if more than one side of the element lies along the boundary of the plate (corner nodes). The extension to these cases is straight-forward.

Free and simply supported edges

Consequently with the approximation in Eq.(44) the line integrals along the side Γ_{ij} of the terms appearing on the right hand side of Eq.(11) will be evaluated as

$$\int_{l_{ij}} n_x \frac{\partial w}{\partial x} d\Gamma = y_{ij} \left[\bar{b}_i^{(e)}, \bar{b}_j^{(e)}, \bar{b}_k^{(e)}, 0, 0, 0\right] \mathbf{a}^{(e)} \tag{45}$$

$$\int_{l_{ij}} n_y \frac{\partial w}{\partial y} d\Gamma = -x_{ij} \left[\bar{c}_i^{(e)}, \bar{c}_j^{(e)}, \bar{c}_k^{(e)}, 0, 0, 0\right] \mathbf{a}^{(e)} \tag{46}$$

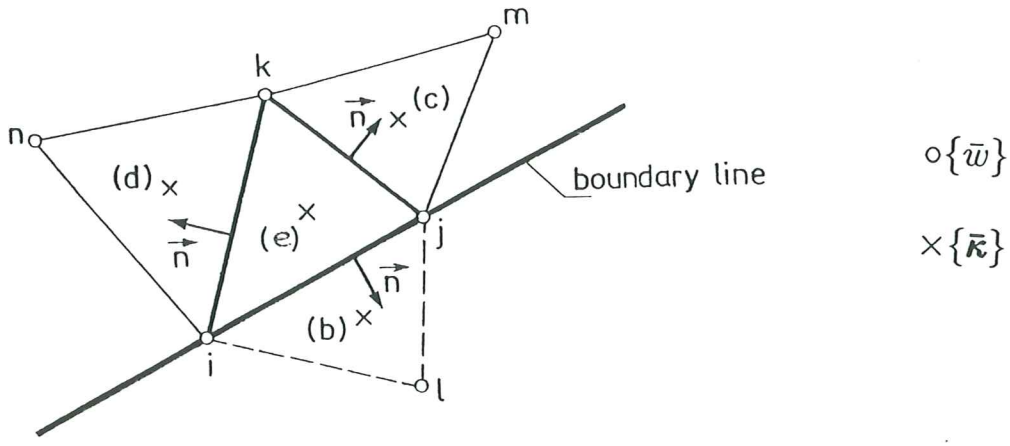

Figure 7 Triangular element lying along a boundary line

instead of using the expressions of Eqs. (37) and (38).

The derivation of matrix $\mathbf{H}^{(e)}$ for this case is again straight-forward and its explicit form is given in Table 1.b.

The conditions for a simply supported edge are simply obtained using this modified $\mathbf{H}^{(e)}$ matrix and constraining the corresponding deflection degrees of freedom to a zero value. This can be done at the global equations solution level in the standard fashion [12].

Remark 11. The conditions of zero bending moments and zero equivalent shear forces along a side (free edge) are natural in this formulation, as it derives from the PVW [12], [13].

Fictitious symmetry edge

If the fictitious symmetry edge lies along a line parallel to the global y axis the symmetry condition is simply

$$\frac{\partial w}{\partial x}\Big|_{\Gamma_{ij}} = 0 \tag{47}$$

and the corresponding terms on the right hand side of Eq. (45) have to be zeroed. This is simply accomplished by setting $\bar{b}_i^{(e)} = \bar{b}_j^{(e)} = \bar{b}_k^{(e)} = 0$ in all the terms where these coefficients appear when evaluating the contribution of side Γ_{ij} to matrix $\mathbf{H}^{(e)}$. The corresponding $\mathbf{H}^{(e)}$ matrix can be then easily evaluated and its explicit form is given in Table 1.c.

If the fictitious symmetry edge lies along a line parallel to the global x axis then the symmetry condition is

$$\frac{\partial w}{\partial y}\Big|_{\Gamma_{ij}} = 0 \tag{48}$$

and this is enforced by making $\bar{c}_i^{(e)} = \bar{c}_j^{(e)} = \bar{c}_k^{(e)} = 0$ in all the terms where these

coefficients appear when evaluating the contribution of side Γ_{ij} to matrix $\mathbf{H}^{(e)}$ (see for instance Eq. (46)).

Clamped edge

If the boundary edge is clamped the conditions that must be satisfied are

$$w\|_{\Gamma_{ij}} = 0 \tag{49}$$

$$\frac{\partial w}{\partial n}\|_{\Gamma_{ij}} = 0 \tag{50}$$

where n is the direction normal to the boundary Γ_{ij}. Condition (49) can be imposed at equation solution level as in the simply supported case. If this condition holds, it is also true that

$$\frac{\partial w}{\partial s}\|_{\Gamma_{ij}} = 0 \tag{51}$$

where s is the direction parallel to Γ_{ij}. Now, considering Eqs.(50) and (51) together one can simply write

$$\nabla w|_{\Gamma_{ij}} = \nabla w^{(e)}|_{\Gamma_{ij}} = \mathbf{0} \tag{52}$$

Then it is obvious that the corresponding $\mathbf{H}^{(e)}$ matrix will be constructed as on Eq.(27), but disregarding the contribution from side Γ_{ij}. (Its explicit form is given in Table 1.d.)

EVALUATION OF STRESS RESULTANTS

The constant bending moment distribution within each single DOF triangle is obtained by the standard expression

$$\mathbf{m}^{(e)} = \mathbf{D}\mathbf{B}^{(e)}\mathbf{a}^{(e)} \tag{53}$$

where matrix $\mathbf{B}^{(e)}$ is given by Eq.(30)

The computation of shear forces is not so straight-forward. The relationship between shear forces and bending moments is given by

$$\mathbf{q} = \left\{ \begin{array}{c} Q_x \\ Q_y \end{array} \right\} = \left[\begin{array}{ccc} \frac{\partial}{\partial_x} & 0 & \frac{\partial}{\partial_y} \\ 0 & \frac{\partial}{\partial_y} & \frac{\partial}{\partial_x} \end{array} \right] \left\{ \begin{array}{c} M_x \\ M_y \\ M_{xy} \end{array} \right\} = \hat{\mathbf{L}}\mathbf{m} \tag{54}$$

The sign criterion for shear forces is shown in Figure 2.

A procedure to evaluate the shear forces is to smooth the discontinuous bending moment field and then to apply Eq.(54) to the resulting continuous field.

An alternative procedure is to use a similar methodology to that used to approximate the curvature field. Thus, integrating Eq.(54) over each element domain gives

$$\int\int_{A^{(e)}} \mathbf{q} dA = \int\int_{A^{(e)}} \hat{\mathbf{L}} \mathbf{m} dA = \int_{\Gamma^{(e)}} \mathbf{T}^T \mathbf{m} d\Gamma \tag{55}$$

Choosing now a constant interpolation for the shear forces within each element as $\mathbf{q} = \mathbf{I}_2 \hat{\mathbf{q}}^{(e)}$, gives

$$\hat{\mathbf{q}}^{(e)} = \frac{1}{A^{(e)}} \int_{\Gamma^{(e)}} \mathbf{T}^T \mathbf{m} dA \tag{56}$$

Eq.(56) requires the evaluation of the bending moments along the element sides. This can be done for the discontinuous bending field case by simple averaging of the corresponding bending moment values contributed by the two adjacents elements sharing each side.

Obviously, the case of a continuous bending field poses no difficulty and Eq.(56) can be directly applied to give the shear forces within each element.

EXAMPLES

The efficiency of the BPT element presented is assessed through different examples of application.

Simply supported square plate under uniform and point loads

The geometry of the plate is shown in Figure 8 where some of the meshes used for the analysis are shown.

A quarter of the plate has been discretized only for symmetry reasons. Note that only structured meshes have been used in this case with the two orientations shown in the Figure 8.

Numerical results for the central deflection, the central bending moment $M_x = M_y$ and the corner vertical reaction for the uniform load case are shown in Table 2 for meshes of 5×5, 10×10, 20×20, and 30×30 BPT elements in a quarter of plate (for symmetry reasons) and the two different mesh orientations shown in Figure 8. Good convergence to the theoretical exact values [11] is obtained in all cases.

Figure 9 shows the convergence plots for the central deflection, the central bending moment and the corner reaction versus the number of degrees of freedom involved in each solution. Numerical results obtained by Batoz et al. [14] using the standard DKT element are also shown for comparison.

The results for the point load case are shown in Table 3 where the convergence of the central deflection and the corner reaction values is shown again for the two

mesh orientations considered. Good results are also obtained in this case with the BPT element.

Figure 10 shows the convergence plots for the central deflection and the corner reaction. The results compare well with those obtained by Batoz et al. [14] using the DKT element also shown in the same figure.

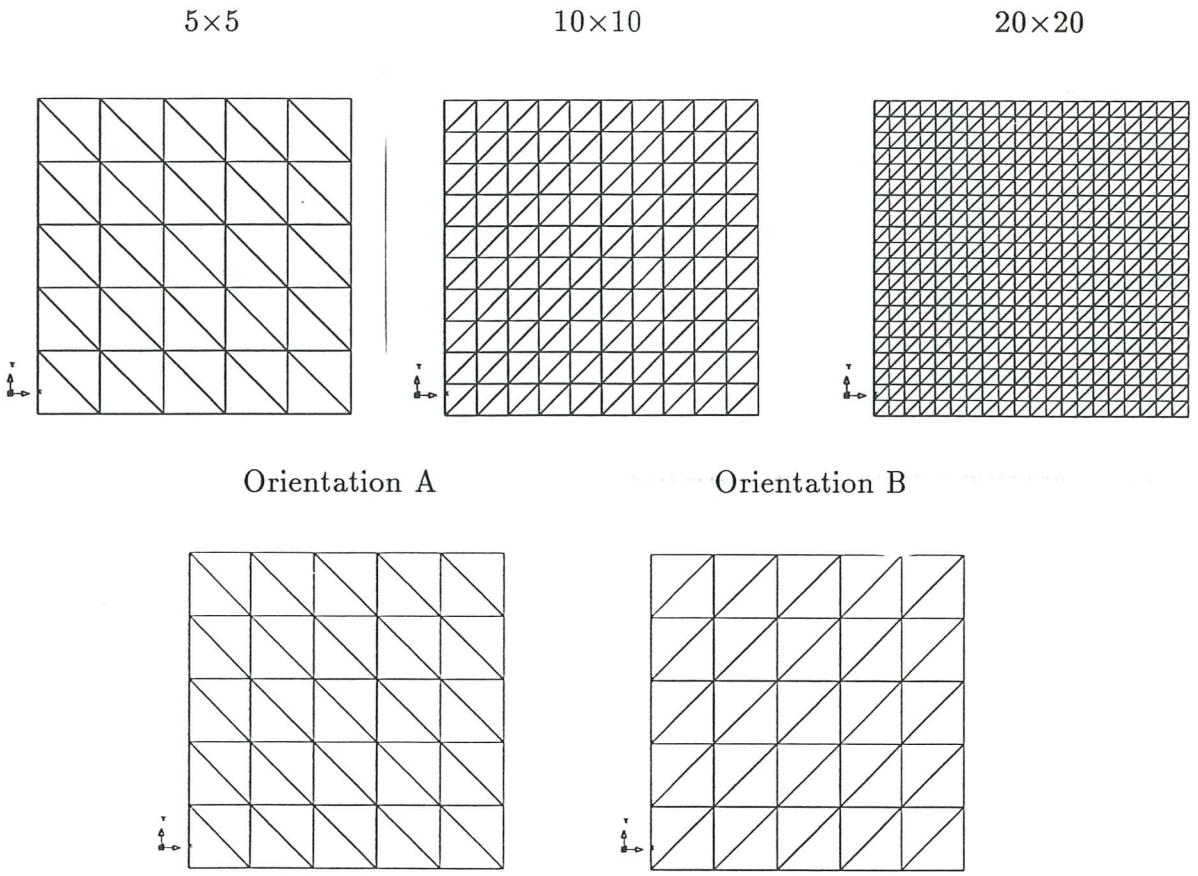

Figure 8 Square plate. Different meshes used in a quarter of plate for symmetry. Mesh orientations A and B

Clamped square plate under uniform and point loads

The second example corresponds to the analysis of the same plate of the previous example with clamped edges.

Numerical results for the central deflection, the central bending moment and the mid-side moment under uniform load for different meshes are shown in Table 4.

The convergence plots of these values is shown in Figure 11 for the purpose of comparison with the DKT results for the same problem [14].

Table 5 shows the results for the central deflection and the mid-side moment for different meshes. The same values are plotted in Figure 12 where results obtained using the DKT element are also shown [14]. Convergence plots shown in Figure 12 indicate that the 3 DOF plate triangle proposed is less sensitive to mesh orientation than the DKT element.

Circular plates under uniform loading

The geometry of the circular plate is shown in Figure 13 together with the different meshes used.

Numerical results obtained for the simply supported and clamped cases are shown in Table 6.a and 6.b.

Excellent results are obtained with relatively coarse meshes for both the central deflections and the central bending moments as it can be seen in these Tables.

Mesh 1 (96 DOF) Mesh 2 (341 DOF) Mesh 3 (736 DOF)

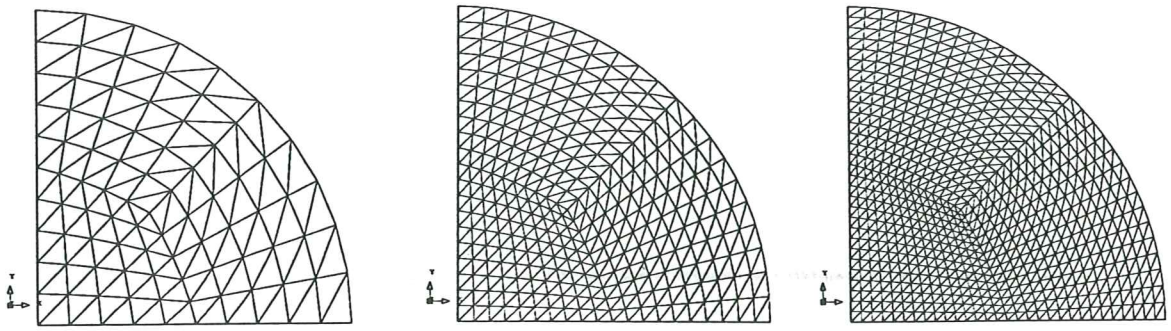

Figure 13 Circular plate. Different meshes used in a quarter of plate for symmetry

CONCLUDING REMARKS

A general methodology for deriving thin plate elements with only a translational degree of freedom has been presented. The methodology can be applied to derive new single nodal degree of freedom plate elements of triangular and quadrilateral shapes with different approximations. The efficiency of the simple 3 DOF triangle proposed has been shown with different examples of applications. This element (termed BPT) has a promising future for more complex plate and shell problems involving dynamics and nonlinear effects.

One of the key issues of the proposed approach lays in the evaluation of the deflection gradient along the element sides. Indeed other more accurate techniques than the simple derivative averaging procedure used in this paper could be used to enhance the element approximation. Among these special finite difference energy techniques [15], derivative recovery procedures [16] or diffuse element methods [17] could be effectively combined with the approach proposed in this paper for enhanced derivative computation leading to improvements in the BPT element performance.

ACKNOWLEDGEMENTS

The autors are grateful to Prof. O. C. Zienkiewicz for many useful comments during the development of this work.

REFERENCES

1. Uguraz, A. C., *Stresses in plates and shells*, Mc. Graw Hill, 1981.
2. Barnes, M. R., "Form finding and analysis of tension space structure by dynamic relaxation", *Ph. D. Thesis*, Dpt. of Civil Engineering, The City University, London, 1977.
3. Hampshire, J. K. and Topping, B. H. V., "Three node triangular elements with one degree of freedom per node " *Eng. Comput.* **9**, 49-62, 1992.
4. Phaal, R. and Calladine, C. R., "A simple class of finite elements for plate and shell problems. I: Elements for beams and thin plates" *Int. J. Num. Meth. Engng.*, **35**, 955-77, 1992.
5. Phaal, R. and Calladine, C. R., "A simple class of finite elements for plate and shell problems. II: An element for thin shells with only translational degrees of freedom", *Int. J. Num. Meth. Engng.* **35**, 979-96, 1992.
6. Patankar, S. V., *Numerical heat transfer and fluid flow*, Series in Computational Methods in Mechanics and Thermal Sciences, W. J. Minkowycz and E. M. Sparrow (Eds.), Hemisphere Publishing Co., 1980.
7. Hirsch, C., *Numerical computations of internal and external flow*, Vol. I, J. Wiley, 1989.
8. Zienkiewicz, O. C. and Oñate, E., "Finite elements versus finite volumes. Is there really a choice?". Published in *Non Linear Computational Mechanics. State of the Art.* P. Wriggers and R. Wagner (Eds.), Springer Verlag, 1991.
9. Oñate, E., Cervera, M. and Zienkiewicz, O. C., "A study of the finite volume method for structural mechanics ", Research Report **15**, CIMNE, Barcelona, 1992. Submitted to *Int. J. Num. Meth. Engng.*
10. Idelsohn, S. and Oñate, E., "Finite elements and finite volumes for CFD. Two good friends". Research Report **15**, CIMNE, Barcelona, (1992). Submitted to *Int. J. Num. Meth. Engng.*
11. Timoshenko, S., *Theory of plates and shells*, Mc. Graw Hill, 1979.
12. Zienkiewicz, O. C. and Taylor, R. L., *The finite element method*, 4th Edition, Mc. Graw Hill, Vol. I, 1990 and Vol. II, 1991.
13. Oñate, E., *The finite element method for structural analysis*, CIMNE Barcelona, 1993.
14. Batoz, J. L., Bathe, K. J. and Ho, L. W., "A study of three node triangular plate bending elements", *Int. J. Num. Meth. Engng*, **28**, 533-60, 1989.
15. Pavlin, V. and Perrone, N., "Finite difference energy techniques for arbitrary meshes applied to linear plate problems", *Int. J. Num. Meth. Engng.*, **14**, 647-69, 1979.
16. Zienkiewicz, O. C.and Zhu, J. Z., "Superconvergence derivative recovery Techniques and a posteriori error estimator in the FFM", Part I: "General superconvergent recovery Technique", Internal Report CR/672/91, Univ. College of Swansea 1991, to be published in *Int. J. Num. Mesth. Engng.*
17. Nayroles, B., Touzot, G. and Villon, P., "Generalizing the finite element method –Diffuse approximation and diffuse elements" *Comput. Mechanics*, **10**, 307-18, 1992.

APPENDIX

Let us assume the following interpolations for the actual deflection and curvatures and their respective virtual fields

$$\begin{aligned} w &= \mathbf{N}_w \bar{\boldsymbol{w}} \quad , \quad \delta w = \bar{\mathbf{N}}_w \delta \bar{\boldsymbol{w}} \\ \boldsymbol{\kappa} &= \mathbf{N}_\gamma \bar{\boldsymbol{\kappa}} \quad , \quad \delta \boldsymbol{\kappa} = \mathbf{N}_\gamma \delta \bar{\boldsymbol{\kappa}} \end{aligned} \tag{A.1}$$

Substitution of (A.1) in the equilibrium equation (5) and the weighted form of the curvature–deflection relationship (2a) (for both the actual and virtual fields) leads to

$$\int_\Omega \delta \bar{\boldsymbol{\kappa}}^T \mathbf{N}_\gamma^T \mathrm{m} d\Omega = \int_\Omega \delta \bar{\boldsymbol{w}}^T \mathbf{N}_w^T q d\Omega \tag{A.2a}$$

$$\left[\int_\Omega \mathbf{W}_1^T \mathbf{N}_\gamma d\Omega\right] \bar{\boldsymbol{\kappa}} = \left[\int_\Omega \mathbf{W}_1^T \mathbf{L}(\mathbf{N}w) d\Omega\right] \bar{\boldsymbol{w}} \tag{A.2b}$$

$$\left[\int_\Omega \mathbf{W}_2^T \mathbf{N}_\gamma d\Omega\right] \delta \bar{\boldsymbol{\kappa}} = \left[\int_\Omega \mathbf{W}_2^T \mathbf{L}(\mathbf{N}w) d\Omega\right] \delta \bar{\boldsymbol{w}} \tag{A.2c}$$

Choosing now $\mathbf{W}_1 = \mathbf{W}_2 = \mathbf{I}_3$ and integrating by parts the integrals of the *r.h.s.* of (A.2b) and (c) leads to

$$\mathbf{P} \bar{\boldsymbol{\kappa}} = \mathbf{H} \bar{\boldsymbol{w}} \tag{A.3a}$$

$$\mathbf{P} \delta \bar{\boldsymbol{\kappa}} = \mathbf{H} \delta \bar{\boldsymbol{w}} \tag{A3.b}$$

where $\mathbf{P}_{ij} = \int_{\Gamma_i} \mathbf{I}_3 N_{\gamma_j} d\Gamma$ and

$$\mathbf{H}_{ij} = \oint_{\Gamma_i} \mathbf{T}(\nabla N_{w_j}) d\Gamma \tag{A.3}$$

with $\mathbf{T}$ as defined in (9).

Substituting $\delta \bar{\boldsymbol{\kappa}}$ from (A.3b) in (A.2a) gives, after elliminating the virtual displacements,

$$\left[\int_\Omega \mathbf{B}^T \mathbf{D} \mathbf{N}_\gamma d\Omega\right] \bar{\boldsymbol{\kappa}} = \int_\Omega \mathbf{N}_w^T \mathbf{q} d\Omega \tag{A.4}$$

with

$$\mathbf{B} = \mathbf{N}_\gamma \mathbf{P}^{-1} \mathbf{H} \tag{A.5}$$

Eqs.(A.3a) and (A.4) form a system of equations which can be written in matrix form as

$$\begin{bmatrix} \mathbf{P} & -\mathbf{H} \\ \mathbf{A} & 0 \end{bmatrix} \begin{Bmatrix} \bar{\boldsymbol{\kappa}} \\ \bar{\boldsymbol{w}} \end{Bmatrix} = \begin{Bmatrix} 0 \\ \mathbf{f} \end{Bmatrix} \tag{A.6}$$

where

$$\mathbf{A} = \int_{\Omega} \mathbf{B}^T \mathbf{D} \mathbf{N}_{\gamma} d\Omega \qquad (A.7a)$$

$$\mathbf{f} = \int_{\Omega} \mathbf{N}_w^T \mathbf{q} d\Omega \qquad (A.7b)$$

Solution of (A.6) will only exist if the following condition is satisfied

$$n_{\bar{\kappa}} \geq n_{\bar{w}} \qquad (A.8)$$

i.e., the number of $\bar{\boldsymbol{\kappa}}$ variables is greater than that of available nodal deflections (after discounting prescribed values).

The proof of (A.8) can be found in [12]. A simple heuristic evidence of (A.8) can be deduced by noting that $n_{\bar{w}} > n_{\bar{\kappa}}$ would simply imply that the curvatures $\bar{\boldsymbol{\kappa}}$ can be directly deduced from (A.4) by selecting the appropriate number of rows of $\mathbf{A}$ giving a square matrix. This would obviously lead to multiple options for obtaining $\bar{\boldsymbol{\kappa}}$ and to wrong solutions.

Solution of (A.6) can, in fact, be attempted in a two step approach. First the nodal curvatures are obtained from the first row as

$$\bar{\boldsymbol{\kappa}} = \mathbf{P}^{-1} \mathbf{H} \bar{w} \qquad (A.9)$$

Substitution of (A.9) in the second row gives (noting that $\mathbf{P}$ and $\mathbf{H}$ are independent of the coordinates)

$$\mathbf{K} \bar{w} = \mathbf{f} \qquad (A.10)$$

where

$$\mathbf{K} = \mathbf{A} \mathbf{P}^{-1} \mathbf{H} \qquad (A.11)$$

It can be easily shown that the form of matrix $\mathbf{K}$ given above coincides with that of Eq.(21a)

(1)

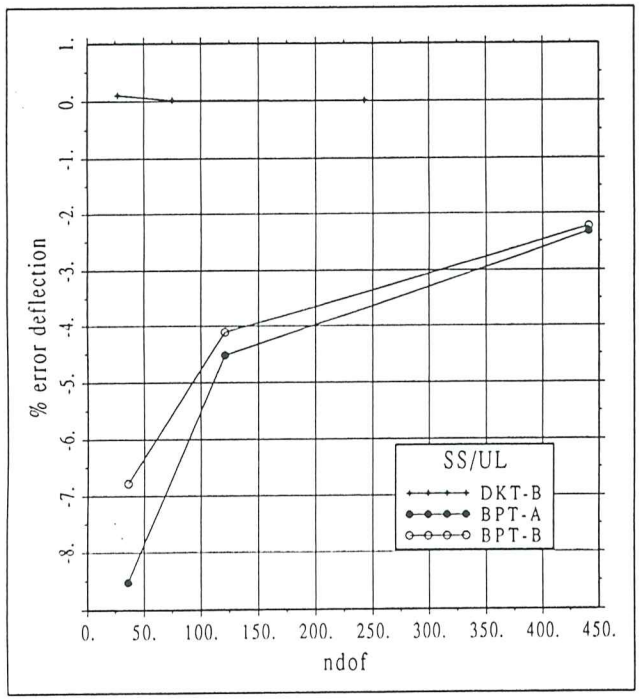

(2)

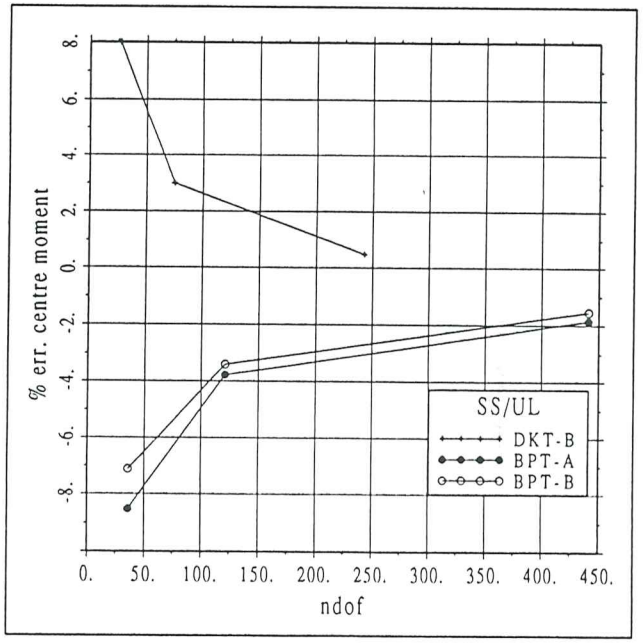

(3)

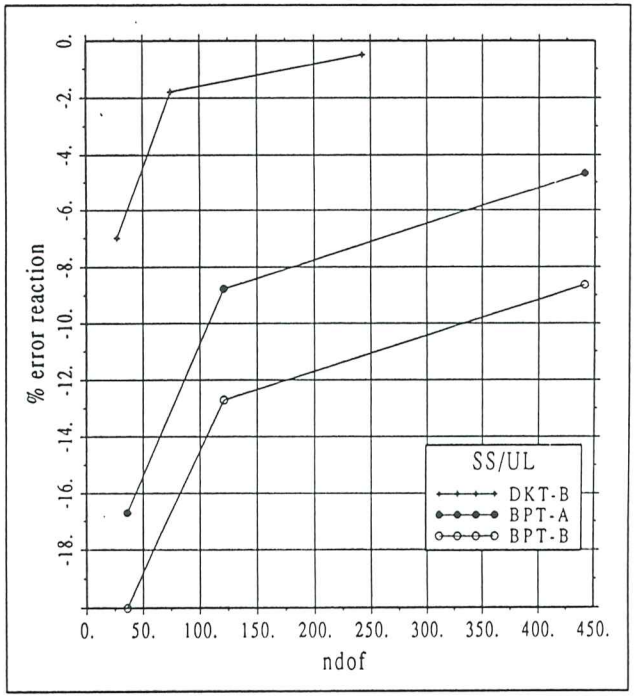

Figure 9 Simple supported square plate under uniform loading. Convergence plots for the central deflection (1), central bending moment (2) and corner reaction (3), for mesh orientations A and B of Figure 8

(1)

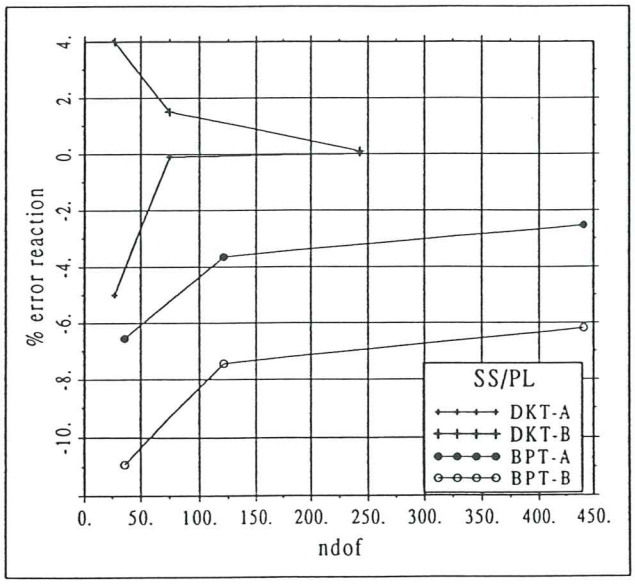

(2)

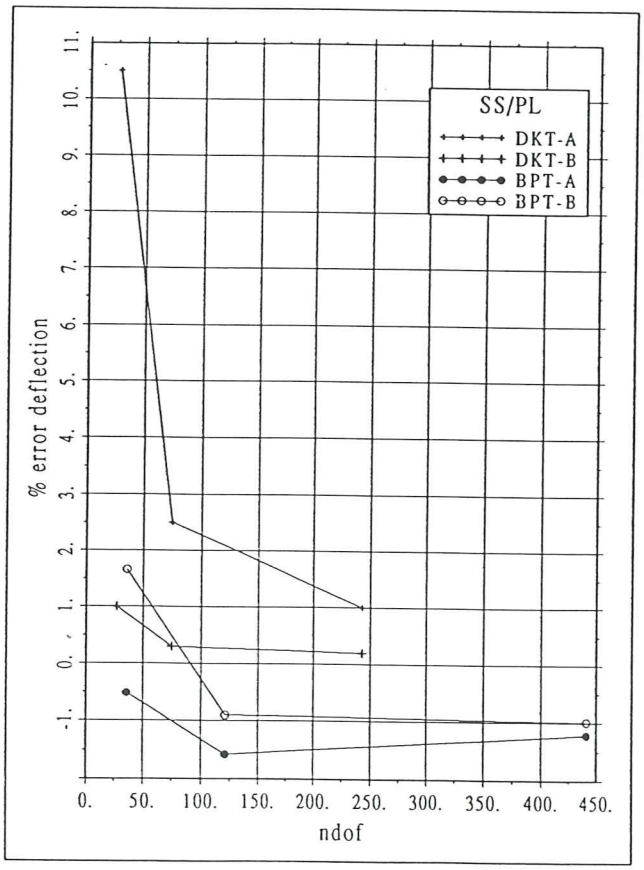

Figure 10 Simple supported square plate under central point load. Convergence plots of central deflection (1) and corner reaction (2) for the two mesh orientations A and B shown in Figure 8

(1)

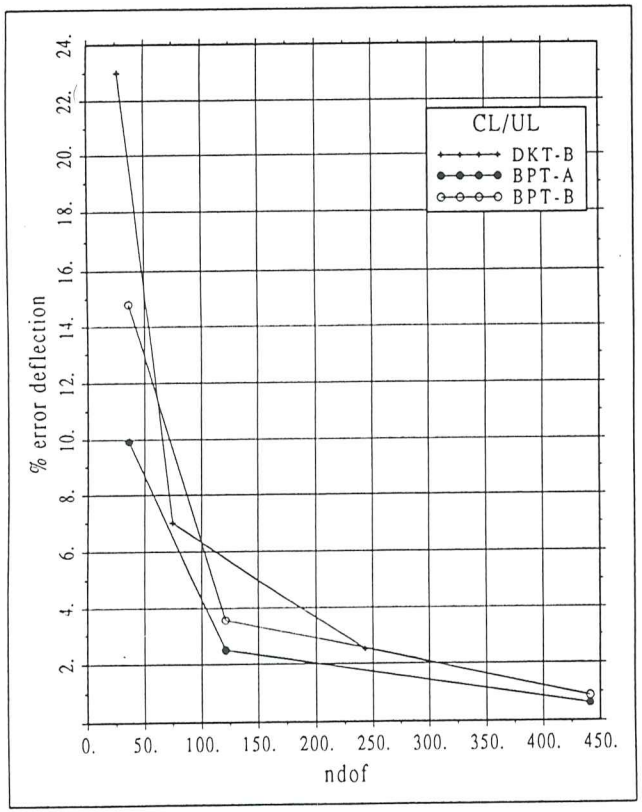

(2)

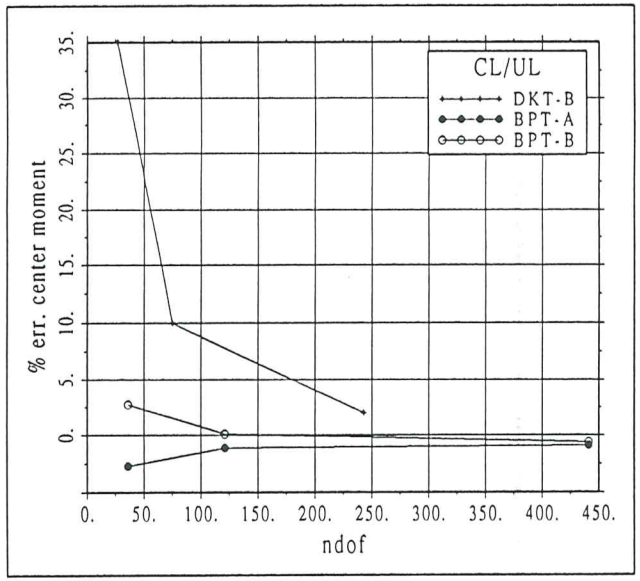

(3)

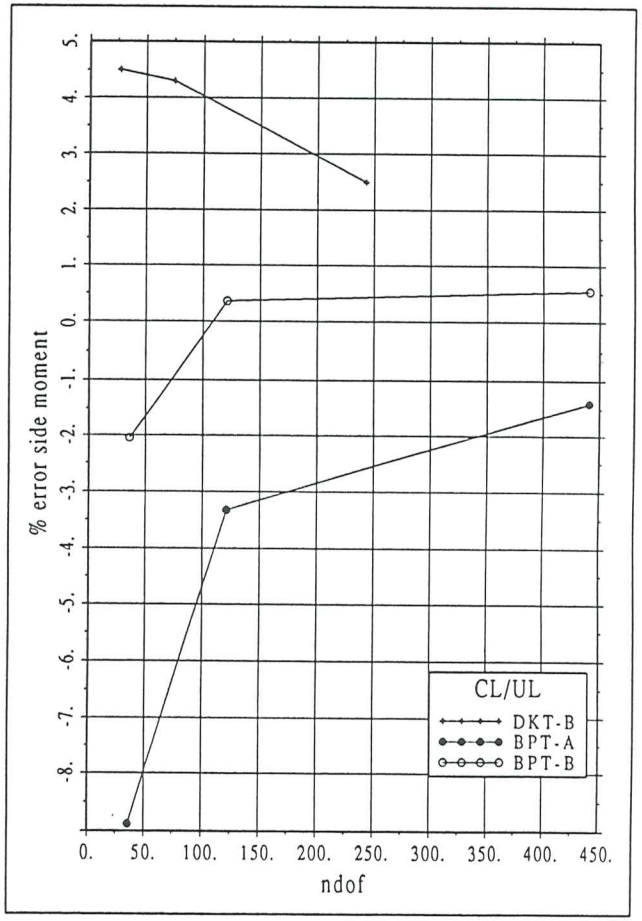

Figure 11 Clamped square plate under uniform loading. Convergence plots for the central deflection (1), the central bending moment (2) and the mid-side bending moment (3) for the two mesh orientations A and B shown in Figure 8

(1)

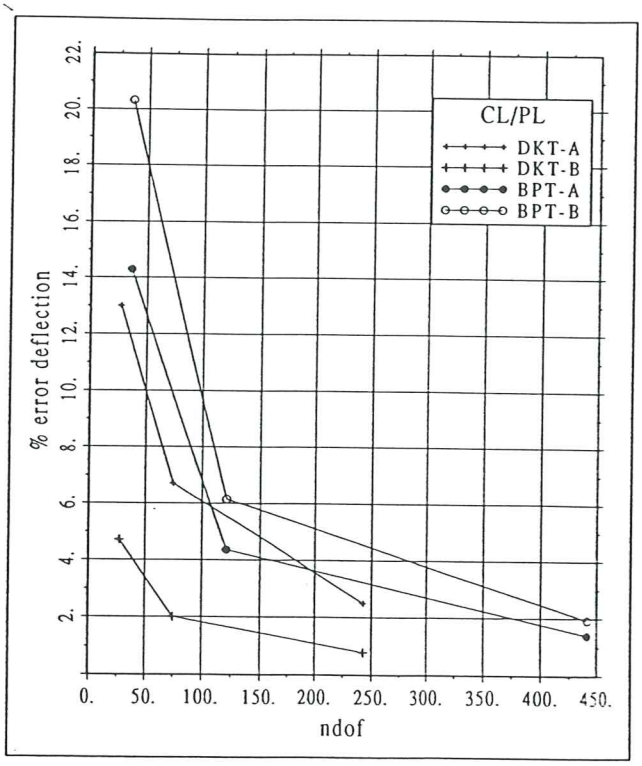

(2)

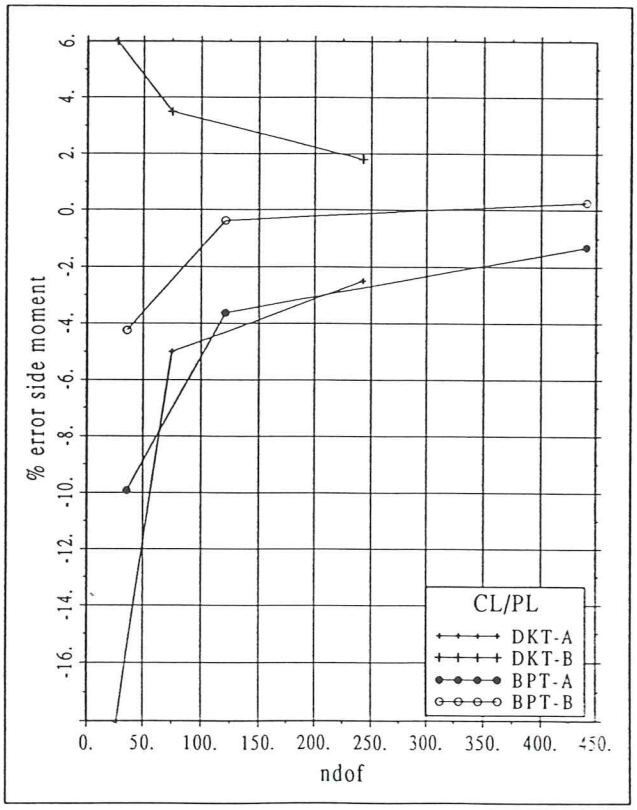

Figure 12 Clamped square plate under point loading. Convergence plots of central deflection (1) and mid-side bending moment (2) for the two mesh orientations A and B shown in Figure 8

$$
\mathbf{H}^{(e)} = \frac{1}{2}\begin{bmatrix}
y_{ij}\bar{b}_i^{(b)} + y_{ki}\bar{b}_i^{(d)} & y_{ij}\bar{b}_j^{(b)} + y_{jk}\bar{b}_j^{(c)} & y_{jk}\bar{b}_k^{(c)} + y_{ki}\bar{b}_k^{(d)} & y_{ij}\bar{b}_l^{(b)} & y_{jk}\bar{b}_m^{(c)} & y_{ki}\bar{b}_n^{(d)} \\
-x_{ij}\bar{c}_i^{(b)} - x_{ki}\bar{c}_i^{(d)} & -x_{ij}\bar{c}_j^{(b)} - x_{jk}\bar{c}_j^{(c)} & -x_{jk}\bar{c}_k^{(c)} - x_{ki}\bar{c}_k^{(d)} & -x_{ij}\bar{c}_l^{(b)} & -x_{jk}\bar{c}_m^{(c)} & -x_{ki}\bar{c}_n^{(d)} \\
y_{ij}\bar{c}_i^{(b)} - x_{ij}\bar{b}_i^{(b)} + & y_{ij}\bar{c}_j^{(b)} - x_{ij}\bar{b}_j^{(b)} + & y_{jk}\bar{c}_k^{(c)} - x_{jk}\bar{b}_k^{(c)} + & y_{ij}\bar{c}_l^{(b)} - x_{ij}\bar{b}_l^{(b)} & y_{jk}\bar{c}_m^{(c)} - x_{jk}\bar{b}_m^{(c)} & y_{ki}\bar{c}_n^{(d)} - x_{ki}\bar{c}_n^{(d)} \\
+y_{ki}\bar{c}_i^{(d)} - x_{ki}\bar{b}_i^{(d)} & +y_{jk}\bar{c}_j^{(c)} - x_{jk}\bar{b}_j^{(c)} & +y_{ki}\bar{c}_k^{(d)} - x_{ki}\bar{c}_k^{(d)} & & &
\end{bmatrix}
$$

$$
\text{with} \qquad \bar{b}_i^{(e)} = \frac{b_i^{(e)}}{2A^{(e)}} \;\; , \;\; \bar{c}_i^{(e)} = \frac{c_i^{(e)}}{2A^{(e)}} \;\; , \;\; \text{etc.}
$$

Table 1.a Matrix $\mathbf{H}^{(e)}$ for the 3 DOF Basic Plate Triangle (BPT)

$$
\mathbf{H}^{(e)} = \frac{1}{2}\begin{bmatrix}
y_{ij}\bar{b}_i^{(e)} + y_{ki}\bar{b}_i^{(d)} & y_{ij}\bar{b}_j^{(e)} + y_{jk}\bar{b}_j^{(c)} & y_{ij}\bar{b}_k^{(e)} + y_{jk}\bar{b}_k^{(c)} + & 0 & y_{jk}\bar{b}_m^{(c)} & y_{ki}\bar{b}_n^{(d)} \\
 & & +y_{ki}\bar{b}_k^{(d)} & & & \\
-x_{ij}\bar{c}_i^{(e)} - x_{ki}\bar{c}_i^{(d)} & -x_{ij}\bar{c}_j^{(e)} - x_{jk}\bar{c}_j^{(c)} & -x_{ij}\bar{c}_k^{(e)} - x_{jk}\bar{c}_k^{(c)} - & 0 & -x_{jk}\bar{c}_m^{(c)} & -x_{ki}\bar{c}_n^{(d)} \\
 & & -x_{ki}\bar{c}_k^{(d)} & & & \\
y_{ij}\bar{c}_i^{(e)} - x_{ij}\bar{b}_i^{(e)} + & y_{ij}\bar{c}_j^{(e)} - x_{ij}\bar{b}_j^{(e)} + & y_{ij}\bar{c}_k^{(e)} - x_{ij}\bar{b}_k^{(e)} + & 0 & y_{jk}\bar{c}_m^{(c)} - x_{jk}\bar{b}_m^{(c)} & y_{ki}\bar{c}_n^{(d)} - x_{ki}\bar{c}_n^{(d)} \\
+y_{ki}\bar{c}_i^{(d)} - x_{ki}\bar{b}_i^{(d)} & +y_{jk}\bar{c}_j^{(d)} - x_{jk}\bar{b}_j^{(d)} & +y_{jk}\bar{c}_k^{(c)} - x_{jk}\bar{c}_k^{(c)} + & & & \\
 & & +y_{ki}\bar{c}_k^{(d)} - x_{ki}\bar{c}_k^{(d)} & & &
\end{bmatrix}
$$

Table 1.b Matrix $\mathbf{H}^{(e)}$ for the 3 DOF Basic Plate Triangle (BPT) with a side ij free or simply supported

$$\mathbf{H}^{(e)} = \frac{1}{2}\begin{bmatrix} y_{ki}\bar{b}_i^{(d)} & y_{jk}\bar{b}_j^{(c)} & y_{jk}\bar{b}_k^{(c)} + y_{ki}\bar{b}_k^{(d)} & 0 & y_{jk}\bar{b}_m^{(c)} & y_{ki}\bar{b}_n^{(d)} \\ -x_{ki}\bar{c}_i^{(d)} & -x_{jk}\bar{c}_j^{(c)} & -x_{jk}\bar{c}_k^{(c)} - x_{ki}\bar{c}_k^{(d)} & 0 & -x_{jk}\bar{c}_m^{(c)} & -x_{ki}\bar{c}_n^{(d)} \\ y_{ij}\bar{c}_i^{(e)} + & y_{ij}\bar{c}_j^{(e)} + & y_{ij}\bar{c}_k^{(e)} + & 0 & y_{jk}\bar{c}_m^{(c)} - x_{jk}\bar{b}_m^{(c)} & y_{ki}\bar{c}_n^{(d)} - x_{ki}\bar{c}_n^{(d)} \\ +y_{ki}\bar{c}_i^{(d)} - x_{ki}\bar{b}_i^{(d)} & +y_{jk}\bar{c}_j^{(d)} - x_{jk}\bar{b}_j^{(d)} & +y_{jk}\bar{c}_k^{(c)} - x_{jk}\bar{c}_k^{(c)} + & & & \\ & & +y_{ki}\bar{c}_k^{(d)} - x_{ki}\bar{c}_k^{(d)} & & & \end{bmatrix}$$

Table 1.c Matrix $\mathbf{H}^{(e)}$ for the 3 DOF Basic Plate Triangle (BPT) with a side ij corresponding to a symmetry boundary parallel to the y-axis

$$\mathbf{H}^{(e)} = \frac{1}{2}\begin{bmatrix} y_{ki}\bar{b}_i^{(d)} & y_{jk}\bar{b}_j^{(c)} & y_{jk}\bar{b}_k^{(c)} + y_{ki}\bar{b}_k^{(d)} & 0 & y_{jk}\bar{b}_m^{(c)} & y_{ki}\bar{b}_n^{(d)} \\ -x_{ki}\bar{c}_i^{(d)} & -x_{jk}\bar{c}_j^{(c)} & -x_{jk}\bar{c}_k^{(c)} - x_{ki}\bar{c}_k^{(d)} & 0 & -x_{jk}\bar{c}_m^{(c)} & -x_{ki}\bar{c}_n^{(d)} \\ y_{ki}\bar{c}_i^{(d)} - x_{ki}\bar{b}_i^{(d)} & y_{jk}\bar{c}_j^{(d)} - x_{jk}\bar{b}_j^{(d)} & y_{jk}\bar{c}_k^{(c)} - x_{ki}\bar{c}_k^{(c)} + \\ & & +y_{ki}\bar{c}_k^{(d)} - x_{ki}\bar{c}_k^{(d)} & 0 & y_{jk}\bar{c}_m^{(c)} - x_{jk}\bar{b}_m^{(c)} & y_{ki}\bar{c}_n^{(d)} - x_{ki}\bar{c}_n^{(d)} \end{bmatrix}$$

Table 1.d Matrix $\mathbf{H}^{(e)}$ for the 3 DOF Basic Plate Triangle (BPT) with side ij clamped

SIMPLY SUPPORTED SQUARE PLATE UNIFORM LOAD						
	CENTRAL DEFLECTION		CENTRAL MOMENT		CORNER REACTION	
MESH	A	B	A	B	A	B
5×5	0.7925-02	0.8076-02	5.4773	5.5416	6.7674	6.4969
10×10	0.8272-02	0.8307-02	5.7614	5.7651	7.4118	7.0948
20×20	0.8462-02	0.8470-02	5.8773	5.8756	7.7443	7.4369
30×30	0.8527-02	0.8531-02	5.9138	5.9095	7.8615	7.5634
Exact [11]	0.8664-02	0.8664-02	5.9875	5.9875	8.125	8.125

$E = 2.0 + 06 \quad \nu = 0.3 \quad t = 0.2 \quad a = 5.0 \quad q = 5.0$

Table 2 Simple supported square plate under uniform loading. Numerical results obtained using the 3 DOF triangle with meshes of two different orientations A and B (Figure 8)

SIMPLY SUPPORTED SQUARE PLATE UNDER POINT LOAD				
	CENTRAL DEFLECTION		CORNER REACTION	
MESH	A	B	A	B
5×5	0.1969-02	0.2012-02	1.0841	1.0136
10×10	0.1947-02	0.1961-02	1.1391	1.0852
20×20	0.1955-02	0.1959-02	1.1744	1.1281
30×30	0.1961-02	0.1963-02	1.1880	1.1435
Exact [11]	0.1979-02	0.1979-02	1.219	1.219

$E = 2.0 + 06 \quad \nu = 0.3 \quad t = 0.2 \quad a = 5.0 \quad P = 10.0$

Table 3 Simple supported square plate under central point load. Numerical results obtained using the 3 DOF triangle with meshes of two different orientations A and B (Figure 8)

CLAMPED SQUARE PLATE UNDER UNIFORM LOAD						
	CENTRAL DEFLECTION		CENTRAL MOMENT		CORNER REACTION	
MESH	A	B	A	B	A	B
5×5	0.2965-02	0.3099-02	2.8097	2.9665	-5.8427	-6.2811
10×10	0.2765-02	0.2794-02	2.8550	2.8900	-6.1985	-6.4349
20×20	0.2715-02	0.2722-02	2.8614	2.8700	-6.3224	-6.4472
30×30	0.2705-02	0.2709-02	2.8624	2.8663	-6.3561	-6.4427
Exact [11]	0.2698-02	0.2698-02	2.8875	2.8875	-6.4125	-6.4125

$E = 2.0 + 06 \quad \nu = 0.3 \quad t = 0.2 \quad a = 5.0 \quad q = 5.0$

Table 4 Clamped square plate under uniform load. Numerical results obtained using the 3 DOF triangle with meshes of two different orientations A and B (Figure 8)

CLAMPED SQUARE PLATE UNDER POINT LOAD				
	CENTRAL DEFLECTION		MIDI-SIDE MOMENT	
MESH	A	B	A	B
5×5	0.1091-02	0.1149-02	-1.1323	-1.2036
10×10	0.9971-03	0.1014-03	-1.2112	-1.2523
20×20	0.9689-03	0.9739-03	-1.2406	-1.2603
30×30	0.9629-03	0.9654-03	-1.2475	-1.2607
Exact [11]	0.9555-03	0.9555-03	-1.257	-1.257

$E = 2.0 + 06 \quad \nu = 0.3 \quad t = 0.2 \quad a = 5.0 \quad q = 5.0 \quad P = 10$

Table 5 Clamped square plate under point load. Numerical results obtained using the 3 DOF triangle with meshes of two different orientations A and B (Figure 8)

a) SIMPLY SUPPORTED				
MESH	DOF	w_0	M_r^0	M_t^0
1	96	39105.4	5.0186	5.0186
2	341	39518.2	5.1075	5.1075
3	736	39611.5	5.1275	5.1275
Exact [11]		39813.7	5.1562	5.1562

b) CLAMPED				
MESH	DOF	w_0	M_r^0	M_t^0
1	96	9914.84	1.9820	1.9820
2	341	9790.91	2.0147	2.0147
3	736	9768.17	2.0219	2.0219
Exact [11]		9765.62	2.0312	2.0312

$E = 10.92 \quad \nu = 0.3 \quad t = 0.1 \quad R = 5.0 \quad q = 1.0$

Table 6 Circular plate under uniform loading. Results for a simple supported (a) and clamped (b) plate